Journal of Structural Geology 33 (2011) 487–499

Contents lists available at ScienceDirect

Journal of Structural Geology

journal homepage: www.elsevier.com/locate/jsg

Influence of stratigraphic setting and simple shear on layer-bound compaction faults offshore Mauritania

Mark T. Ireland*, Neil R. Goulty, Richard J. Davies

Centre for Research into Earth Energy Systems (CeREES), Department of Earth Sciences, Durham University, South Road, Durham DH1 3LE, United Kingdom

ARTICLE INFO

Article history:
Received 2 August 2010
Received in revised form
8 November 2010
Accepted 17 November 2010
Available online 24 November 2010

Keywords:
Antithetic faults
Offshore Mauritania
Polygonal faults
Simple shear

ABSTRACT

We have used three-dimensional seismic data to examine the geometry of layer-bound compaction faults on the Mauritanian continental margin. The faults deform a fine-grained Neogene unit which mantles buried canyons. Above the canyons, most layer-bound faults strike perpendicular to the canyon axes, whereas adjacent to the canyons the faults are omni-directional and intersect bedding planes in polygonal patterns. On the flanks of a large structural high, faults also strike perpendicular to the slope direction, displaying a concentric pattern. Faults that show preferential alignment are located in areas with increased bedding dip, and most aligned faults are antithetic to the bedding dip. Where the bedding dip is greater than ~1°, the synthetic faults dip more steeply than the antithetic faults. This discovery was unexpected because the stress tensor due to the effect of gravity on a dipping margin would cause the antithetic faults to form with steeper dips, which we show theoretically. We hypothesise that the layer hosting the faults has been subjected to simple shear of ~20° or more, with the top of the layer displaced downdip by ~100 m relative to its base. A potential application of these, and similar, observations is to assess slope stability on continental margins.

1. Introduction

Sediments are subject to body and surface forces, including gravity, from the time of deposition and their response to these forces depends on their mechanical properties and the magnitudes of the forces (Maltman, 1994). Numerous authors have identified that depositional slopes can influence the development of faults in sediments (e.g. Crans et al., 1980; Higgs and McClay, 1993; Kobayashi et al., 1998; Victor and Moretti, 2006). The geometry of extensional fault systems is also affected by the presence of low friction substrates which act as basal detachments (e.g. Morley and Guerin, 1996). Of particular relevance to the observations reported here, Stewart and Argent (2000) showed that the kinematics of synthetic versus antithetic fault arrays dictate that synthetic fault arrays must branch onto a basal detachment, whereas faults within antithetic arrays may die out downwards.

Layer-bound systems of compaction faults found in fine-grained sedimentary units commonly comprise networks of normal faults with strike directions that form polygonal geometries on bedding planes (Cartwright and Dewhurst, 1998). Bedding plane geometries of compaction fault systems may depart from polygonal forms due to the influence of external stresses such as basin-floor slope (e.g. Higgs and McClay, 1993) and tectonic faults (Hansen et al., 2004). Here we describe layer-bound faults from the Neogene succession offshore Mauritania (Fig. 1). Layer-bound fault systems deform a deep marine succession that overlies several kilometre-wide canyons. We document changes in the planform geometry of fault systems above the canyons and on the flanks of a large structural high, and interpret them with reference to the kinematic model of Stewart and Argent (2000) for the development of synthetic and antithetic fault arrays. We then consider the distribution of dips within these layer-bound fault systems in the light of a theoretical analysis of the stress state induced by gravity acting on a dipping margin. In two areas where the continental margin is dipping and both antithetic and synthetic faults are present, we infer that the host layer has undergone a significant amount of simple shear deformation.

2. Layer-bound compaction faults

Factors common to layer-bound systems of normal faults are that they have only been found in low-energy depositional settings, and the host sediments are dominantly composed of very fine-grained lithologies such as smectitic claystones, siliceous or

* Corresponding author. Present address: BP Exploration, Chertsey Road, Sunbury Upon Thames, Middlesex TW16 7LN.
E-mail address: Mark.Ireland@bp.com (M.T. Ireland).

0191-8141/$ – see front matter © 2010 Elsevier Ltd. All rights reserved.
doi:10.1016/j.jsg.2010.11.005

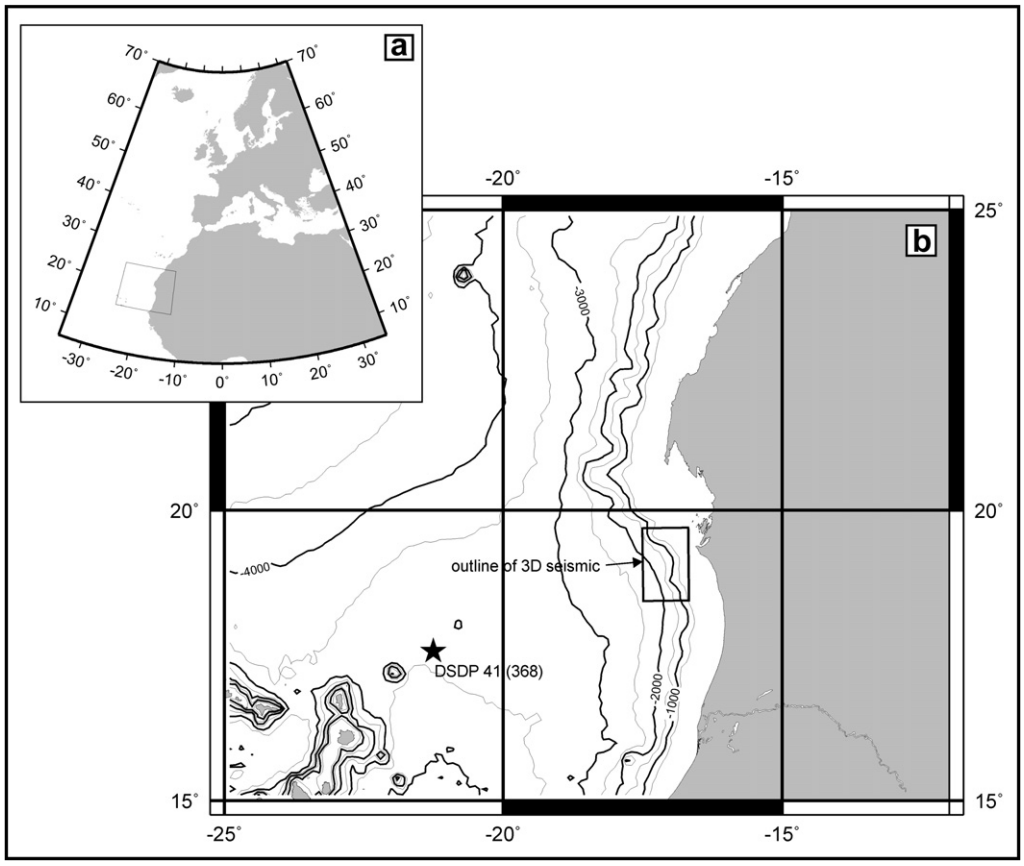

Fig. 1. Location map showing (a) the position of Mauritania on the west African margin and (b) the location of the 3D seismic survey with bathymetry contoured in metres below sea surface. The star marks the position of DSDP 41 (hole 368).

carbonate oozes and chalks, with high porosity and extremely low permeability (Cartwright and Dewhurst, 1998). Such systems have developed over large areas of passive margins and over some intracratonic basins, commonly with the faults cutting stratigraphic horizons in a crudely polygonal geometry. These so-called polygonal fault systems have been identified in more than 50 sedimentary basins world-wide (Cartwright and Dewhurst, 1998). They are widespread on the North Atlantic Margin (Lonergan et al., 1998; Clausen et al., 1999; Lonergan and Cartwright, 1999; Gay and Berndt, 2007; Hustoft et al., 2007), and other notable studies have focused on polygonal fault systems found in Australia (e.g. Watterson et al., 2000), offshore Canada (Hansen et al., 2004) and offshore West Africa (Gay et al., 2004). Polygonal fault systems are thought to have resulted from volumetric reduction with bed-parallel compaction, which complements the heaves on the faults, in addition to vertical compaction (Cartwright and Lonergan, 1996).

Layer-bound polygonal systems of normal faults are an intriguing phenomenon because purely uniaxial compaction of clastic sediments generally does not result in brittle shear failure (Goulty, 2008). Consequently, their very existence in layer-bound sequences that have not undergone tectonic extension seemed paradoxical when they were first identified on three-dimensional (3D) seismic data (Cartwright, 1994). Laboratory measurements (Bishop et al., 1971) and field data (Goulty and Swarbrick, 2005) provide evidence that low coefficients of friction on fault surfaces are the key factor that allows polygonal fault systems to develop (Goulty, 2001, 2002, 2008). Once faults have nucleated in the fine-grained host sediments, they can continue to grow with increasing overburden stress under laterally confined conditions, provided that the coefficient of residual friction on the fault surfaces is sufficiently low.

A small number of layer-bound compaction fault systems have been described where the typically ordered polygonal pattern is disrupted (e.g. Higgs and McClay, 1993; Hansen et al., 2004). Layer-bound faults from the Moray Firth with a dominant dip direction shelfwards were attributed to downslope gravity sliding, triggered by tilting (Higgs and McClay, 1993). Lonergan and Cartwright (1999) studied polygonal faults in the Alba Field, and noted that the density of faulting in the mudrocks was reduced above the reservoir and that 18% of the faults at one horizon had strike directions within a 10° range, parallel to the slope direction. They suggested that stress heterogeneities associated with the change in lithofacies from sand to mud and stress field alterations associated with the compactional draping were responsible for these observations. Hansen et al. (2005) identified that the presence of tectonic faults influenced the organisation of nearby polygonal fault systems, giving rise to orthogonal intersections between the two sets.

3. Effect of seafloor slope on fault geometry

In sedimentary basins where the strata are horizontal, one principal stress axis is vertical and the other two principal stress axes lie in the horizontal plane. In tectonically passive settings, the maximum effective stress σ'_1 is vertical, and stress is isotropic in the horizontal plane. If any normal compaction faults are initiated, there is no preferred strike orientation (Fig. 2a). Where the strata are dipping, with bedding planes parallel to the dipping seafloor,

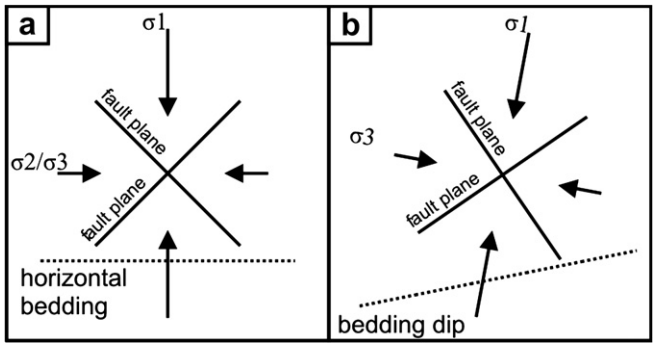

Fig. 2. (a) Effective stresses acting within a tectonically passive basin where the bedding is horizontal. (b) Maximum and minimum effective stresses acting within a tectonically passive basin where the bedding dips to the left.

the effect of gravity modifies the effective stress tensor as shown in Fig. 2b: σ'_1 is increased compared to the case of horizontal strata, and plunges in the downslope direction at a steep angle; the intermediate principal effective stress σ'_2 lies in the strike direction of the strata; and the minimum effective stress σ'_3 is reduced and plunges gently in the upslope direction, orthogonal to σ'_1 (Mandl, 1988, p.121). The preferred strike direction of any normal compaction faults that are initiated is now parallel to the strike of the strata, in the direction of σ'_2. Furthermore, if the faults are antithetic, dipping in the upslope direction, the fault dip is increased; and if the faults are synthetic, dipping in the downslope direction, the fault dip is decreased.

Here we derive the Terzaghi effective stress tensor due to gravity acting on plane-parallel beds of sediment below a planar dipping seafloor, and give a numerical example to illustrate the expected effect on the relative attitudes of any synthetic and antithetic compaction faults that may be initiated in the sediment.

We consider the effective stresses acting on a bedding plane at a general point Q (Fig. 3). The algebraic symbols used are defined as follows:

g: gravitational acceleration,
h: perpendicular depth of Q below seafloor,
K: constant,
X, Y, Z: Cartesian axes with X-axis downslope parallel to the seafloor, Y-axis in the strike direction, and Z-axis perpendicular to the seafloor,
θ: dip of the bedding and the seafloor,
ρ_b: average bulk density between Q and the seafloor,
ρ_w: density of seawater,

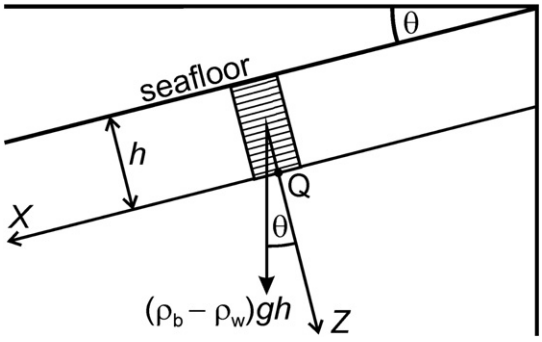

Fig. 3. Effect of gravity at a general point Q in plane-parallel sedimentary layers below a dipping seafloor. The algebraic expression is the difference between the vertical gravitational force acting on unit cross-sectional area of the bedding plane through Q and the hydrostatic pressure at Q.

σ'_1: maximum principal effective stress,
σ'_2: intermediate principal effective stress, and
σ'_3: minimum principal effective stress.

The effective stress tensor at Q is calculated by considering the effect of gravity on the sediment between Q and the seafloor. The vertical force of gravity acting on unit cross-sectional area of the bedding plane through Q exceeds the hydrostatic pressure by $(\rho_b - \rho_w)gh$ and, assuming no overpressure is present, the excess force per unit area may be resolved into a normal effective stress $(\rho_b - \rho_w)gh\cos\theta$ acting in the Z-direction and a shear stress $(\rho_b - \rho_w)gh\sin\theta$ acting in the X-direction.

We assume that the sediment compacts uniaxially, in the direction of the maximum principal stress, the principal effective stresses maintain the same relative magnitudes during compaction, and the strains in the X–Y plane are zero. Then the stress in the X–Y plane must be isotropic, and the normal effective stresses acting in the X-direction and the Y-direction may be expressed as $K(\rho_b - \rho_w)gh\cos\theta$. Provided that the bedding dip is small, it is reasonable to assume that K is approximately equal to the coefficient of earth pressure at rest, which may be taken as a constant for a given lithology (Mayne and Kulhawy, 1982). Furthermore, the Y-direction is a principal stress direction because there are no shear stresses acting in the X–Y and Y–Z planes. Now we need to determine the magnitudes and directions of the principal effective stresses acting in the X–Z plane.

The two-dimensional effective stress tensor referred to (X, Z) coordinate axes is

$$(\rho_b - \rho_w)gh\begin{pmatrix} K\cos\theta & \sin\theta \\ \sin\theta & \cos\theta \end{pmatrix} \tag{1}$$

The eigenvalues of this tensor are the maximum and minimum principal effective stresses, and the corresponding eigenvectors define their directions. They may be found by a standard procedure for square matrices (Stroud and Booth, 2007). The maximum principal effective stress is

$$\sigma'_1 = (\rho_b - \rho_w)gh\left[(1+K)\cos\theta + \sqrt{(1-K)^2\cos^2\theta + 4\sin^2\theta}\right]\Big/2 \tag{2}$$

plunging basinwards at the angle

$$\arctan\left\{\left[(1-K)\cos\theta + \sqrt{(1-K)^2\cos^2\theta + 4\sin^2\theta}\right]\Big/2\sin\theta\right\} + \theta \tag{3}$$

and the minimum principal effective stress is

$$\sigma'_3 = (\rho_b - \rho_w)gh\left[(1+K)\cos\theta - \sqrt{(1-K)^2\cos^2\theta + 4\sin^2\theta}\right]\Big/2 \tag{4}$$

plunging shelfwards at the angle

$$\arctan\left\{2\sin\theta/\left[(1-K)\cos\theta + \sqrt{(1-K)^2\cos^2\theta + 4\sin^2\theta}\right]\right\} - \theta \tag{5}$$

The intermediate principal effective stress is in the Y-direction and has magnitude

$$\sigma'_2 = K(\rho_b - \rho_w)gh\cos\theta \tag{6}$$

As a numerical example, suppose that $K = 0.7$, a typical value for the coefficient of earth pressure at rest in clay (Mayne and Kulhawy,

1982), and $\theta = 3^\circ$. The maximum principal effective stress plunges basinwards at 83.4°. The minimum principal effective stress is 1.3% less than the intermediate principal effective stress and plunges shelfwards at 6.6°. If synthetic and antithetic normal faults form under these stress conditions (Fig. 2), it is to be expected that the dips of the antithetic faults would be 13° steeper than the dips of the synthetic faults.

4. Geological setting

Vear (2005) has provided an excellent account of the petroleum plays of the Mauritanian continental margin, and placed them in their wider geological context. The continental shelf offshore Mauritania (Fig. 1) is a passive margin with significant oil and gas discoveries at Chinguetti and Banda. On the West African margin, deepwater channelised systems are an important petroleum play, with turbidite complexes as exploration targets and proven reservoirs. During the rifting of the Proto-Atlantic Ocean, Liassic evaporites were deposited in the axes of Triassic-Early Jurassic graben. Sediment starvation during the Jurassic allowed the development of carbonate platform complexes, which ceased during the Valangian when a major transgressive event resulted in the deposition of several hundreds of metres of marine shale. During the Albian to Turonian, deepwater conditions predominated on the margin with a wide variety of depositional environments represented. The Campanian to the Maastrictian was a period of relative lowstand during which there was major incision of the continental slope, evident as buried canyons clearly imaged in the seismic data. The Oligocene succession on the margin is dominated by deepwater calcarenites and claystones. From the Early Miocene through to the Recent, canyon systems and a large number of channels have traversed the upper slope.

The layer-bound fault systems investigated here lie within Neogene strata. On the West African margin, the Neogene succession is generally thin, but offshore Mauritania it is significantly thickened with complex deposition from the Late Miocene to the present day (Schwab et al., 2007). There are many slides and mass transport complexes throughout the Neogene succession, and their formation was the consequence of uninterrupted deposition of sediment in an open-slope environment which gave rise to rapid accumulation of poorly consolidated sediment intercalated with thin weak layers (Antobreh and Krastel, 2007). Canyon systems and smaller channels cross and incise the slope at numerous stratigraphic levels throughout the Neogene succession. These canyons may be filled with bathyal turbidites (Vear, 2005) and, further offshore, have fed basin-floor fan systems. Schwab et al. (2007) have identified contourite drifts deposited in channel pathways that can be confused with turbidity current channel levees, and when these deposits become buried they may be even more difficult to distinguish due to loss of seismic resolution with increasing depth.

5. Database and methodology

Data have been interpreted from a single time-migrated 3D seismic reflection volume that covers an area of 4000 km^2 with water depths of ~500–2500 m (Fig. 1). These data were processed using a standard sequence of steps including multiple suppression and post-stack time migration. The survey has a bin size of 25 m × 25 m and the data have a vertical resolution, given by one quarter of the wavelength at the dominant frequency, in the Neogene of about 10 m. The processed data have not been zero-phased. In the seismic sections shown, a reflection event consisting of a red loop followed by a blue loop represents an increase in acoustic impedance downwards.

A generalised depth conversion function, derived from unreleased velocity data in several wells across the Mauritanian margin, was used to convert fault heights from time (ms) to depth (m), and to calculate the dip angle for the faults. Deep Sea Drilling Project (DSDP) velocity data provide further corroboration for the depth conversion, with velocities in the Recent to Neogene clays and claystone lithologies of DSDP Leg 41, Site 368 ranging from 1430 to 2460 m s^{-1} (Trabant, 1977). Assuming an average velocity of 2000 m s^{-1} between the seafloor and the infilled canyons, the seismic sections are displayed here with a vertical exaggeration of ~1.5 over that interval.

Seismic attribute maps were used for the interpretation of faults on selected horizons. We used edge detection and coherency (e.g. Brown, 2005) as the primary method of imaging the faults, as shown by the examples in Fig. 4a and b, but for clarity in this and subsequent figures we show fault trace maps interpreted from these seismic attributes, as in Fig. 4c. Fault dips were calculated from the horizontal and vertical offsets of upper and lower tips at the middle of fault traces on vertical seismic sections oriented perpendicular to the strike of the fault. The regional seismic stratigraphy, which is described in more detail in the next section, is relatively well constrained, although we cannot rule out local variations in the lithology because we have no well data in the area covered by the 3D seismic survey.

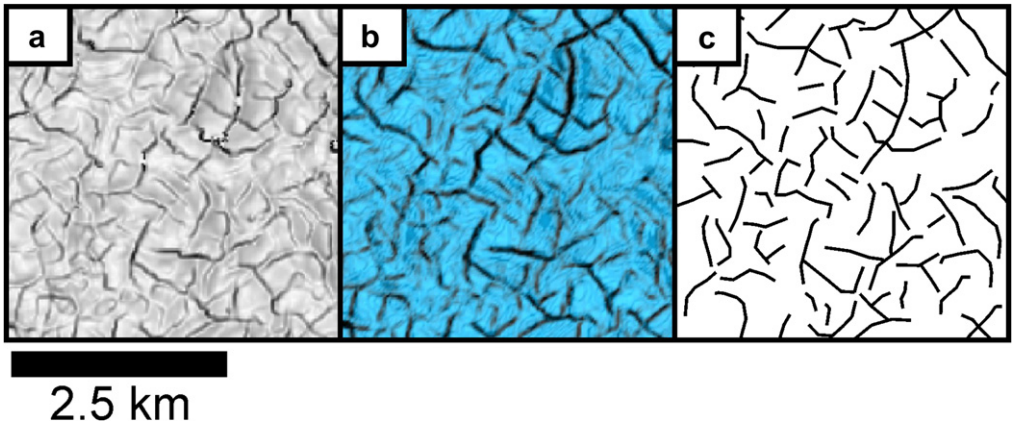

Fig. 4. Horizon slices generated during the interpretation: (a) edge detection map, dark shading highlights steps on the interpreted horizon; (b) coherency volume, dark colours are discontinuous regions, and blue continuous; and (c) interpreted fault traces picked from (a) and (b). (For interpretation of the references to colour in this figure legend, the reader is referred to the web version of this article).

6. Seismic observations

6.1. Regional structural elements

Structural elements that can be recognised on the margin include deep-rooted Mesozoic faults associated with rifting of the proto-Atlantic and shallow collapse faults associated with the ascent of salt diapirs and folding of the overburden. However, only the structural high of the Khop Structure, discussed below, affects the layer-bound fault systems in this study, and there is no evidence of faults that penetrate through the whole Palaeogene succession to cut both Mesozoic and Neogene strata.

In the southern portion of the survey, the dips of the Neogene strata are significantly steepened beyond the regional dip by a large structural high, the Khop Structure (Fig. 5). The structure is ~6 km high, ~60 km in diameter at its base, and ~10 km in diameter at its top. The top is irregular with several circular mounds which protrude up to ~200 m above the top of the main structure. The eastern flank is steeper (maximum dip ~14°), and the western flank is gentler (maximum dip ~6°). The structure has poor internal reflectivity. Reflection events around 4 s two-way time onlap the structure, which suggests an Early Cretaceous age. The origin of the structure is uncertain, but possibilities include a buoyant serpentinite body, mobilised and emplaced diapirically from the upper mantle (cf. Bonatti, 1976). Such serpentinite bodies have been found along large, tectonically active fracture zones which intersect the Mid-Atlantic Ridge (Miyashiro et al., 1969). The circular mounds at the top of the structure are interpreted as carbonate pinnacle reefs (e.g. Elvebakk et al., 2002). Apart from the large excursions from the regional dip due to the Khop Structure, there are local departures due to major periods of canyon incision of the slope.

6.2. Neogene elements

The section marked 'Unit 1' in Fig. 6 is 200–400 m thick and its top and base are marked by reflection events of positive polarity. The unit is characterised by a layered succession of relatively high-amplitude reflection events that are offset by many faults with throws of up to 70 m. Based on the seismic character of Unit 1 and its position within the existing stratigraphic framework, this unit is interpreted as deepwater sediment, mostly likely consisting of hemipelagic siltstones and mudstones and siliceous shales. There is evidence for Unit 1 having a significant biogenic silica component on the basis of a strong reflection with positive polarity that cross-cuts stratigraphic reflections (Fig. 6c), and thus has a character consistent with an opal-A to opal-CT transformation boundary (e.g. Davies and Cartwright, 2002). DSDP Leg 41 also encountered siliceous sediments of a similar age (Riech and Roesch, 1977).

Below Unit 1, a succession of planar parallel reflections is commonly truncated by channel features, interpreted as deepwater canyons (Fig. 6). Within them, the seismic reflectivity is relatively poor. The canyons traverse the survey area from north-east to south-west (Fig. 7). The observed canyon geometries, abrupt incision of the slope, the westward decrease in slope gradient from and locally occurring slumping and gravity-driven deformation indicate that during the Neogene the setting was mid-slope. Eastward is more proximal, and there is evidence to support an upper slope setting, including canyon and channel amalgamation and cannibalisation (e.g. Bouma, 2004). Depositional elements such as channel bodies can generally be mapped out using a variety of amplitude analysis techniques (Brown, 2005), but the identification of internal features within the canyons is difficult here because of the poor reflectivity, which may be due to the high structural dips and complex stacking patterns within the canyons (e.g. Santos et al., 2000).

We have examined the deformation of Unit 1 associated with three canyons in particular, termed canyons I–III. Canyon I has low sinuosity and in cross-section has a maximum width of 5 km, a maximum depth of 300 m, and truncates stratigraphic reflections (Fig. 8). Canyon II has low sinuosity, a maximum width of 8 km, and a maximum depth of 300 m. Upslope it consists of two individual segments that amalgamate, both truncating stratigraphic reflections (Fig. 9). Canyon III also consists of two individual segments which amalgamate. Its course has been deflected around the southern margin of the Khop Structure. It has a maximum width of 4 km and a maximum depth of 250 m (Fig. 10). All three canyons are considered contemporaneous. The three canyons all incise the slope and we have measured the dip of the base of each canyon to be steeper than the incised stratigraphy. These dips are 3° at the base of Canyon I, 2.5° at the base of Canyon II, and 3° at the base of Canyon III. The dip of the strata adjacent to the canyons is <1° (e.g. Fig. 11). Unit 1 was deposited after canyons I and II had been infilled,

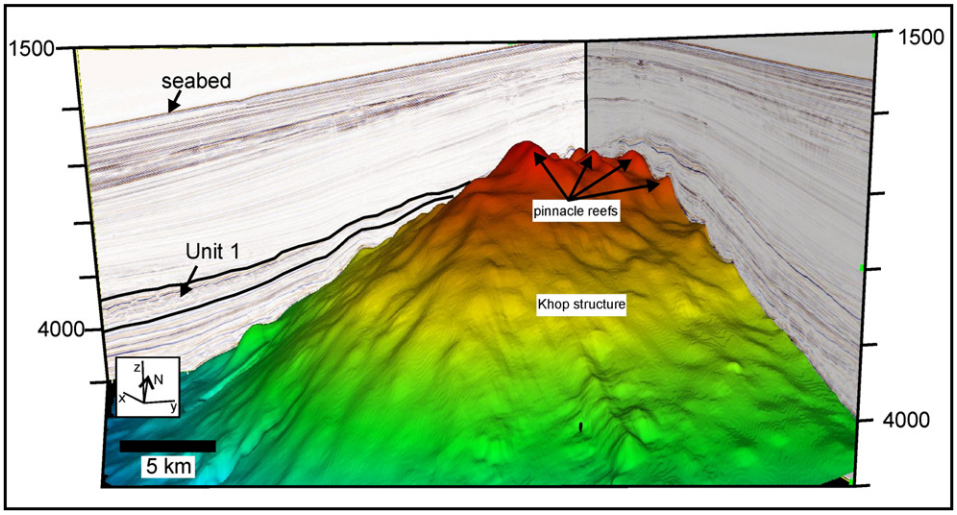

Fig. 5. 3D visualisation of the Khop Structure. The interpreted upper surface of the structure is coloured by two-way time (red shallowest, blue deepest). Unit 1 is the faulted interval. Vertical scale is two-way time in milliseconds. (For interpretation of the references to colour in this figure legend, the reader is referred to the web version of this article).

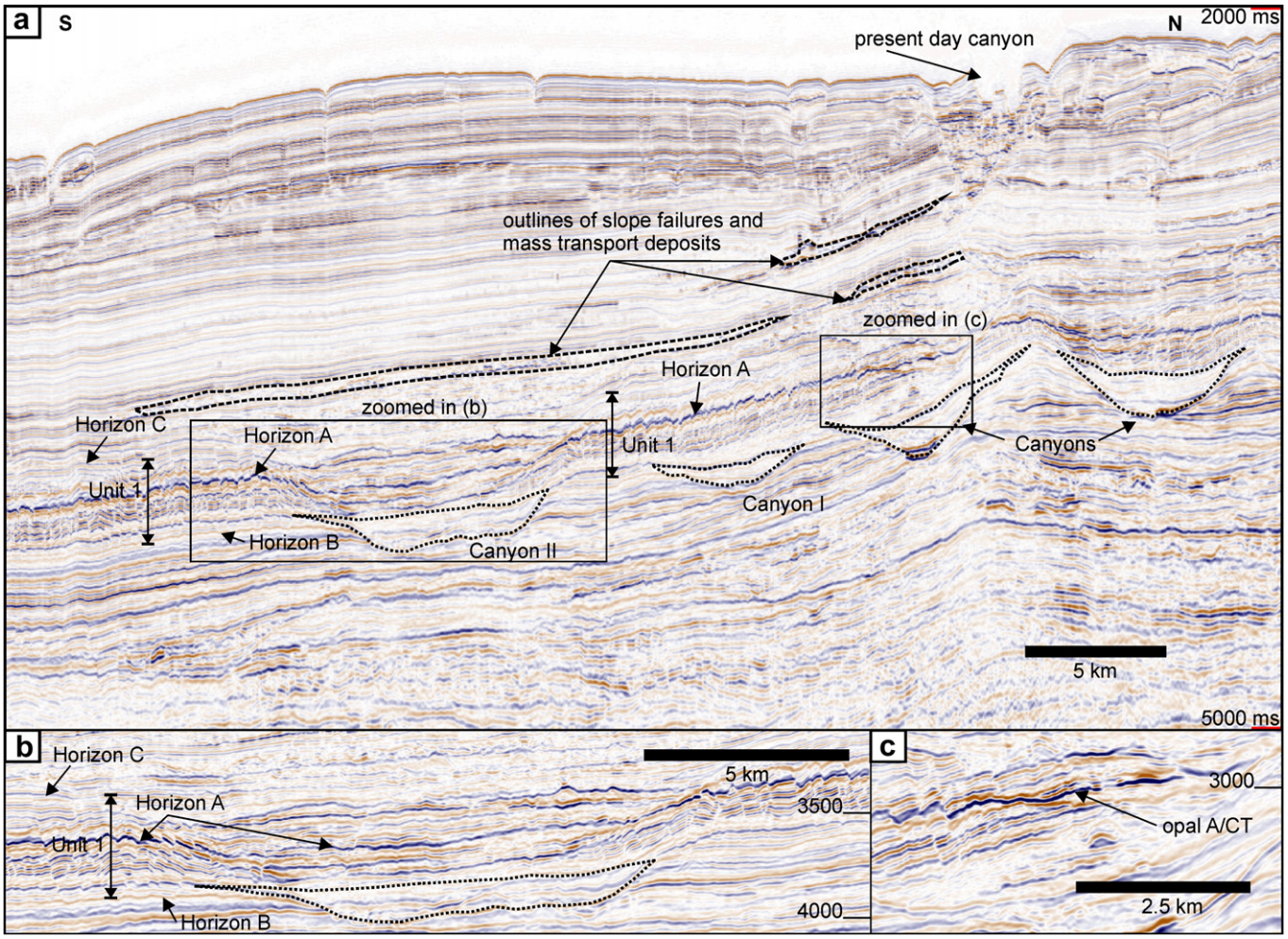

Fig. 6. (a) Representative S–N seismic line showing examples of kilometre-wide canyons which incise the margin, and the overlying Unit 1. Horizon A is the horizon used to interpret fault traces, Horizon B marks the base of Unit 1, and Horizon C marks the top of Unit 1. (b) Zoom to show truncation of seismic reflections by canyon incision and detail of Unit 1. (c) Zoom to show detail of the opal-A/CT reflection where it is prominent. Vertical scale is two-way time in milliseconds. The vertical exaggeration is ~4× in (a) and ~1.5× in (b) and (c).

but forms the fill for Canyon III, where the canyon was bypassed during sandy deposition and later filled during transgression (e.g. Vear, 2005).

6.3. General seismic characteristics of layer-bound fault systems

Layer-bound fault systems intensely deform Unit 1. The faults are exclusively normal faults with dip-slip displacements. Maximum throw values of the faults are in the range 10–100 m, but mostly are in the range 30–70 m. The lower tips of the faults mostly appear to terminate at Horizon B, given the limits of seismic resolution, and the upper tips of many faults are around Horizon C, but some clearly extend above (Fig. 6). The maximum throw of the faults tends to occur around Horizon A. Faults are either planar or slightly listric in cross-section. There are no observable changes in fault plane dip at the inferred opal-A to opal-CT transformation boundary (e.g. Neagu et al., 2010). This may be due to the fact that the porosity drop due to silica diagenesis is only small (<10%) and therefore does not result in a measurable change in fault plane dip. Most faults have mapped segment lengths of 300–2500 m. The planform is polygonal across large areas, but not everywhere. The fault systems exhibit dramatic changes in the distribution of strike directions to a dominant single orientation above canyons I, II and III.

6.4. Layer-bound faulting above canyons

Faults which deform Unit 1 above Canyon I are dominated by a single direction of fault dip, antithetic to the dip of the slope (Fig. 8a). The faults are all normal faults, and typically maximum throws are ~12 m. Faults imaged on vertical seismic sections are generally linear with dips ~30°, assuming an interval velocity of 2000 m s^{-1} for Unit 1. In planform, the fault segments have linear to curvilinear traces and are 300–2500 m long (Fig. 8c). The planform distribution of faults is dominated by parallel to sub-parallel segments, oriented NW–SE and spaced 200–400 m apart. Because of the strong dominant fault trend, fault intersections are uncommon. Above the margins of the canyon, a second fault population is observed, with a dominant NE–SW trend parallel to the canyon axis (Fig. 8c). The faults which are perpendicular to the canyon axis tend to terminate close to the faults along the margins of the canyons.

Faults which deform Unit 1 above Canyon II are also dominated by a single direction of fault dip, antithetic to the dip of the slope (Fig. 9a). The faults are all normal faults, and typically maximum throws are ~20 m. Fault traces are slightly concave to the hanging wall and have dips ~35°, again assuming an interval velocity of 2000 m s^{-1}. The planform distribution of faults is dominated by

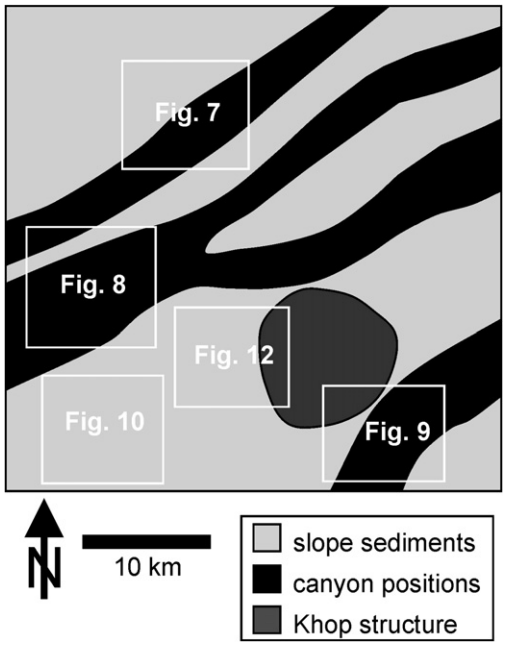

Fig. 7. Line drawing showing the positions of the canyons (in black) which traverse the 3D seismic survey area within the Neogene succession. The positions of the fault maps shown in subsequent figures are outlined in white.

parallel to sub-parallel segments spaced 400–1500 m apart. The dominant orientation of the faults is NW–SE (Fig. 9c), perpendicular to the canyon axis. Because of the strong dominant fault trend, fault intersections are uncommon. Adjacent faults may overlap, and in some instances link laterally along trace. Above the margins of Canyon II there are sets of faults with a dominant NE–SW trend parallel to the canyon axis (Fig. 9c), similar to those observed above the margins of Canyon I but fewer in number. Again the faults which are perpendicular to the canyon axis tend to terminate against the faults above the margins of the canyons.

Canyon III has been infilled by Unit 1, indicating that this canyon was bypassed or abandoned and not filled with sandy sediments. A significant difference in the faulting of Unit 1 here is that in cross-section the faults are both antithetic and synthetic relative to the bedding dip (Fig. 10a). The faults are all normal faults, with a maximum throw of ~15 m. Faults are more noticeably listric than those that deform Unit 1 above canyons I and II. Measurements of fault dips reveal that antithetic faults and synthetic faults have markedly different fault dips. Antithetic faults have a gentler dip of ~30°, while synthetic faults have a steeper dip of ~40°. In planform, the faults are regularly spaced and orientated WNW–ESE, which is again perpendicular to the canyon axis (Fig. 10b). Reflection events tend to bend down towards the fault plane on the hanging wall side, and curve up towards the fault plane on the footwall side (Fig. 10a). There are faults trending NNE–SSW along the canyon margins, including along the line of amalgamation of the two canyon segments, but fewer than seen above the margins of Canyon I.

6.5. Layer-bound polygonal fault systems

Where Unit I does not overlie canyons, the faults display no preferred orientation in map view (Fig. 11). The faults are all normal faults, and typically throws are ~30 m. Examination of fault dips reveals distinct changes depending on the direction of fault dip relative to the slope. Within ~10 km of the Khop Structure, where the bedding dip is between 1° and 1.5°, the antithetic faults have gentler dips around 35° and the synthetic faults have steeper dips around 40°, whereas at greater distances the antithetic and synthetic faults have similar dip distributions (Fig. 12). At fault planes, reflection events may curve down into the fault plane on the hanging wall side, and curve up into the fault plane on the footwall side. The planform distribution of faults is polygonal, with cell

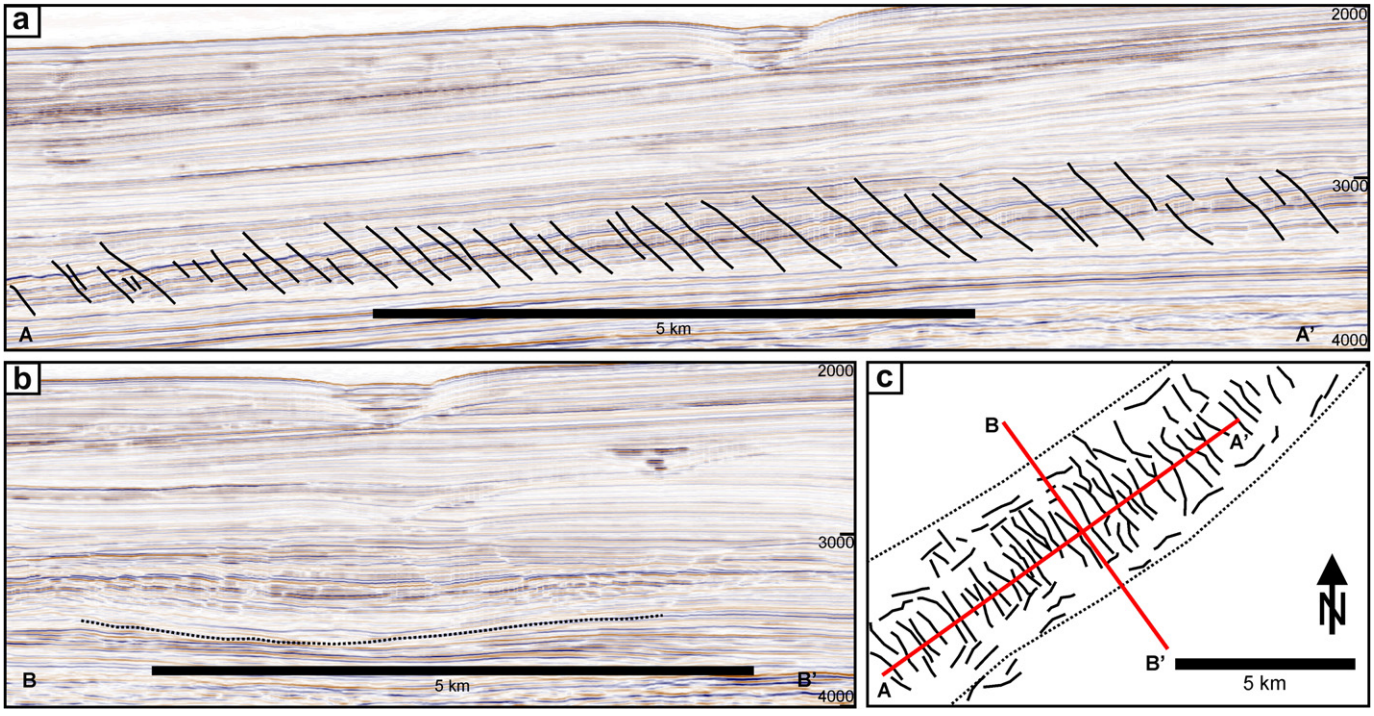

Fig. 8. Representative seismic sections from Canyon I (a) along the axis of the canyon, showing a domino array of antithetic faults, and (b) perpendicular to the canyon axis. (c) Fault trace map showing the two dominant fault trends above the canyon. Canyon base and margins are marked by dotted lines. Vertical scale in (a) and (b) is two-way time in milliseconds.

Fig. 9. Representative seismic sections from Canyon II (a) along the axis of the canyon, showing a domino array of antithetic faults, and (b) perpendicular to the canyon axis. (c) Fault trace map showing the two dominant fault trends above the canyon. Canyon base and margins are marked by dotted lines. Vertical scale in (a) and (b) is two-way time in milliseconds.

diameters in the range 200–1000 m. Fault intersections are commonly orthogonal or at high angles.

6.6. Faults on the flanks of the Khop Structure

Where Unit 1 drapes the flanks of the Khop Structure (Fig. 5), faults show a concentric map pattern around the structure (Fig. 13a). The faults have a linear to curvilinear traces with lengths in the range 1–3 km. This concentric pattern is located at distances of ~5 km from the centre of the structure, where the bedding dip is ~10°. In section, the faults are antithetic relative to the slope (Fig. 13c) and they have very low dip angles of ~20°.

7. Interpretation

7.1. Overview

The layer-bound fault systems described here show varying fault patterns and dip distributions. These variations are interpreted to relate to the 1) presence of underlying stratigraphic elements, i.e. the canyons, 2) variations associated with changes in lithology, and 3) changes in the dip of the bedding. The regional dip measured across the 3D seismic survey is between 0.5° and 3°, generally decreasing basinwards, except on the flanks of the Khop Structure where the dip exceeds 10° in places. The fault kinematics and influence of stratigraphic elements and dip on the fault systems are described in the following sections.

7.2. Aligned arrays versus polygonal arrays

Layer-bound faults above and within canyons and on the flanks of the Khop Structure show preferential orientations and do not display the typical polygonal planform pattern of most layer-bound fault systems. The stress field can therefore not be isotropic in these areas. On the steep flanks of the Khop Structure, the bedding dip is significantly greater (~10°) than the regional dip, and the alignment of the faults is parallel to the strike of the slope. Since the Khop Structure is approximately circular, the fault pattern is concentric. This observed alignment of faults is in accordance with the previous work on the preferential alignment of layer-bound fault systems (e.g. Higgs and McClay, 1993) which has shown that stratigraphic dip of a few degrees results in the intermediate principal effective stress being orientated in the strike direction. The direction of fault dip will again be determined by the nature of the substrate. An alternative explanation for the development of concentric normal faults on the flanks of diapiric structures could

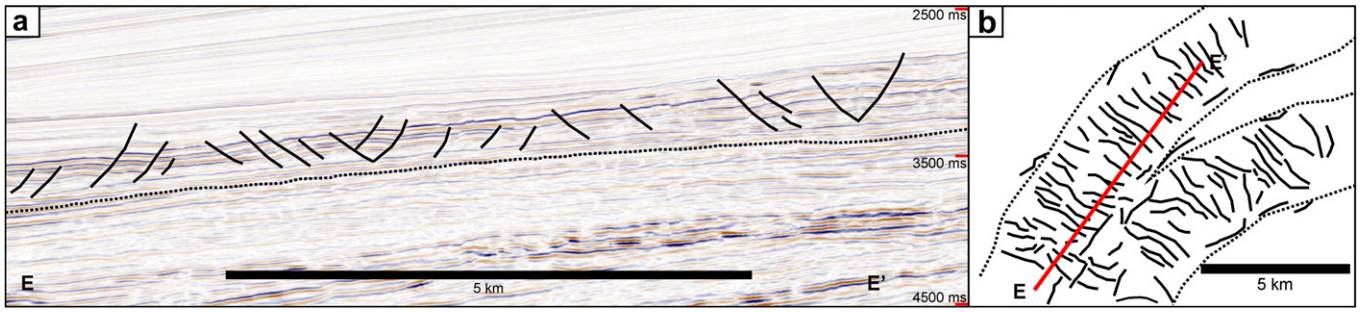

Fig. 10. (a) Representative seismic section from Canyon III showing synthetic and antithetic faults. (b) Fault trace map showing the dominant fault trends. Canyon margins are marked by dotted lines. Vertical scale in (a) is two-way time in milliseconds.

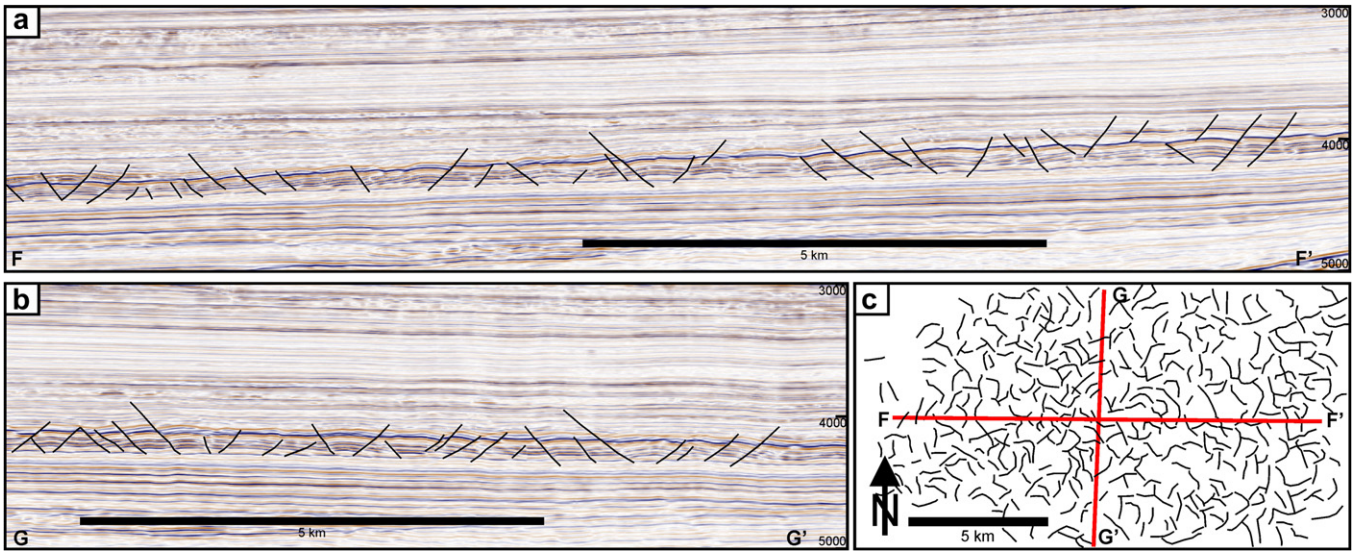

Fig. 11. Representative seismic sections from a polygonally faulted area: (a) section containing the dip direction of the slope; and (b) section along the strike of the slope. (c) Fault trace map. Vertical scale in (a) and (b) is two-way time in milliseconds.

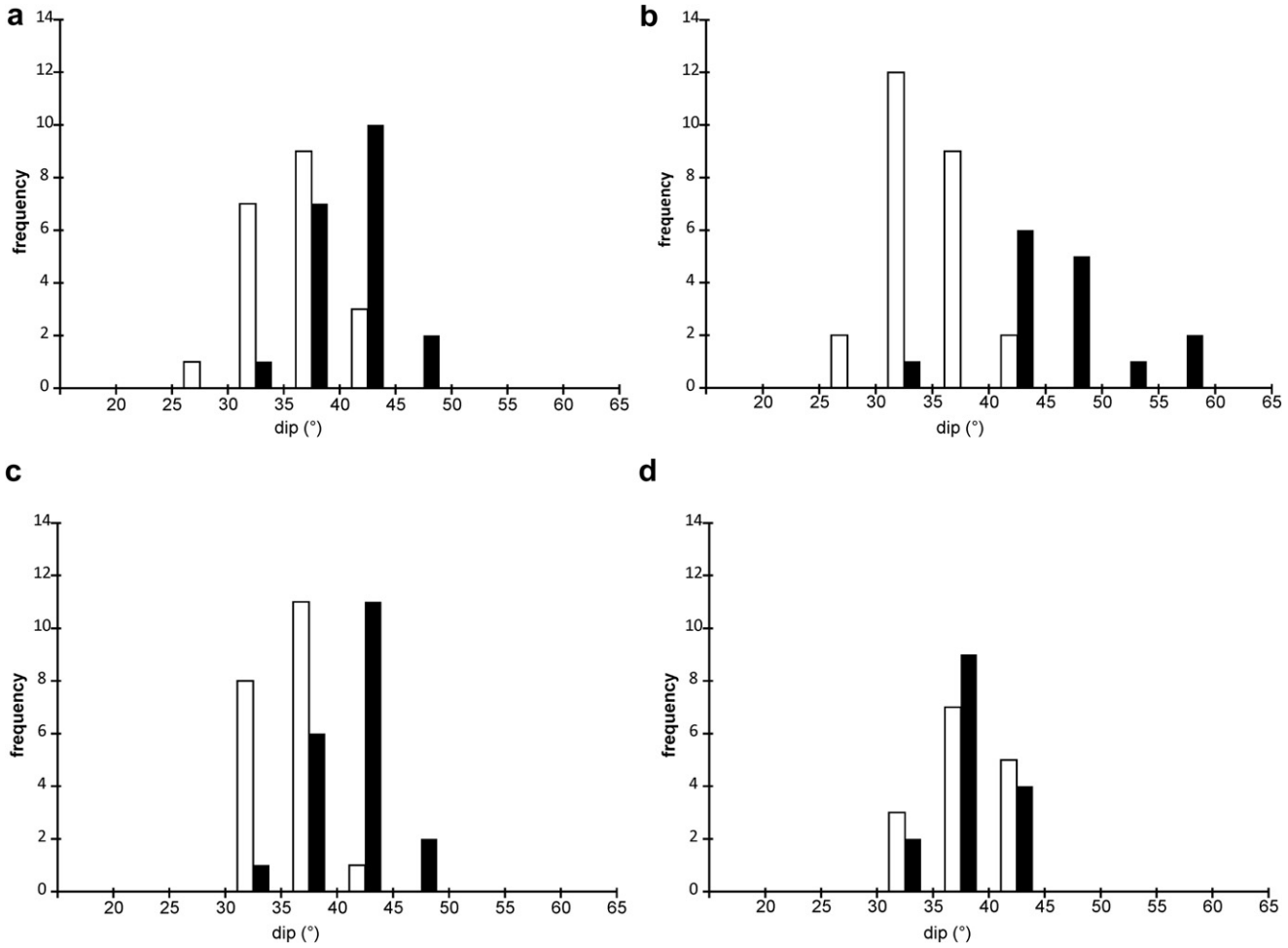

Fig. 12. Histograms of fault dip for: (a) antithetic faults in canyons I (white bars) and II (black bars); (b) antithetic (white bars) and synthetic (black bars) faults in canyon III; (c) antithetic (white bars) and synthetic (black bars) polygonal faults within 10 km of the Khop Structure, with strike directions within 20° of the strike of the slope; and (d) antithetic (white bars) and synthetic (black bars) faults in the polygonal fault systems more than 10 km from the Khop Structure, with strike directions within 20° of the strike of the slope.

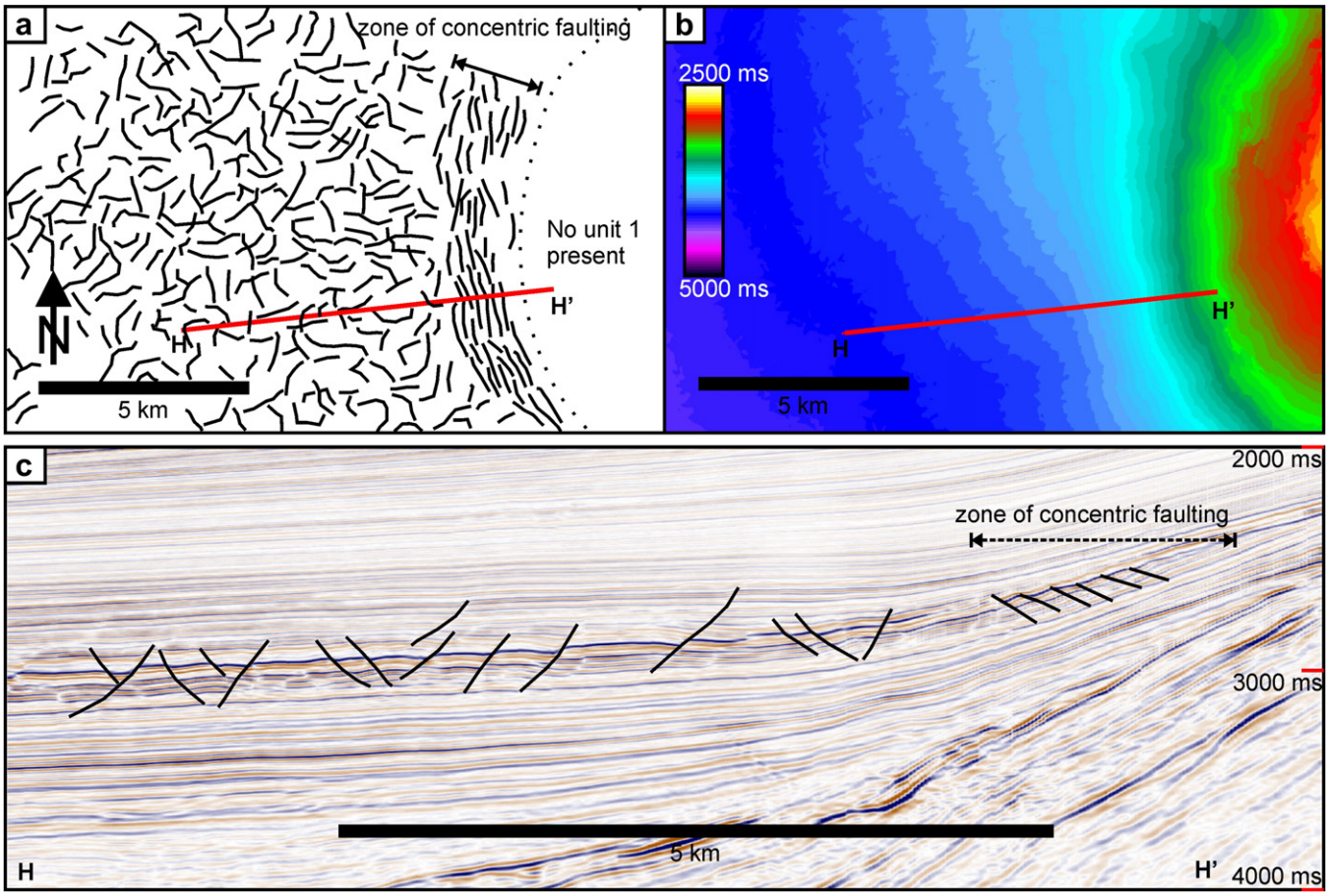

Fig. 13. (a) Fault trace map of Unit 1 close to and on the western flank of the Khop Structure. (b) Time structure map for Horizon A. (c) Seismic section along the profile H–H′ marked in (b).

be that they are extensional faults caused by intrusion, but such faults would be synthetic to the bedding dip (e.g. Stewart, 2006), not antithetic as observed here. Furthermore, from evidence of onlap (Fig. 5), deposition of Unit 1 post-dates the emplacement of the Khop Structure.

Aligned faults above canyons I and II and within Canyon III are perpendicular to the axes of the canyons. Canyons are major erosional features in deepwater settings (Reading, 1998) and, as a result of their incision, the canyon infill has greater dip than the same beds adjacent to the canyons. This increased bedding dip again appears to be the key factor in the alignment of the faults. It is not necessarily the case that only compaction faults with strike directions in this orientation were initiated, but clearly only those faults with this orientation have developed to a seismically resolvable scale. Some of the faults above the margins of the canyons dip towards the canyon axes, while others are antithetic. We attribute their alignment to local horizontal anisotropy induced by some combination of monoclinal drape of the faulted layer across the canyon margins and differential compaction (e.g. Carver, 1968; Cosgrove, 1999; Davies et al., 2009). It is difficult to arrive at a more specific interpretation because of the limited extent and inconsistent dips of these fault subsets.

7.3. Synthetic versus antithetic faults

The fault systems above canyons I and II contain only antithetic domino faults. In such a system, a basal detachment can be ruled out as this would favour the development of faults synthetic to the slope (cf. Stewart and Argent, 2000). In the case of antithetic faulting, the upper parts of fault blocks are allowed to move some distance downdip, through rotation of fault blocks about their lower tips, while remaining in continuity with the upper layer which can also move downdip (Fig. 14a). Where Unit 1 is faulted within Canyon III, faults are both antithetic and synthetic. In this case, there must be a detachment at the base of the faulted interval (Fig. 14b).

The concentric faults on the steepened flanks of the Khop Structure are all antithetic to the slope. In the case of faults being aligned by increased bedding dip, there is no detachment so faults are pinned at the lower tips, as in canyons I and II.

7.4. Evidence for simple shear from fault dips

Histograms of fault dip show that the dips of the faults above Canyon I are smaller than those above Canyon II (Fig. 12a), although the bedding dip of $\sim 2^{\circ}$ above Canyon I is greater than that above Canyon II where it is $\sim 1^{\circ}$. Furthermore, the concentric faults on the flanks of the Khop Structure have extremely low fault dips ($<25^{\circ}$) even though the bedding dip is $\sim 10^{\circ}$, i.e. the fault dips are much gentler than might be expected given that an increase in bedding dip should cause antithetic faults to dip more steeply. In the case of Canyon III, the dips of the synthetic faults are steeper than those of the antithetic faults (Fig. 12b). The same observation is true for the polygonal faults within 10 km of the concentric faults on the Khop Structure (Fig. 12c), but not for the polygonal faults at greater distances (Fig. 12d). The contrasting fault dips in Fig. 12b and c

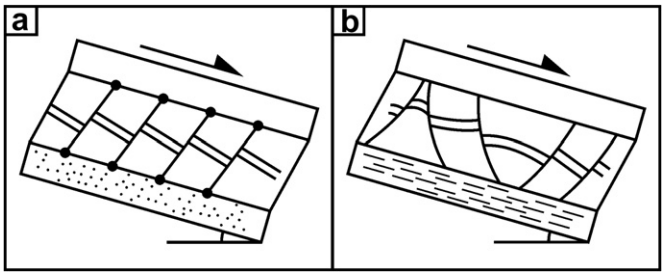

Fig. 14. Cartoons of (a) antithetic faults where there is no basal detachment, and (b) antithetic and synthetic faults where there is a detachment present (after Stewart and Argent, 2000).

cannot be explained by a rotation of the principal stresses, because the effect of downslope gravity traction is to induce exactly the opposite effect on the dips of synthetic and antithetic faults. As shown in Section 3 and Fig. 2, where the bedding is dipping an antithetic fault would form at a steeper dip than the synthetic fault. So we infer that the dips of all these faults have been modified by something other than compaction perpendicular to the bedding since the faults first developed.

There are two possible reasons why the synthetic faults are observed to dip more steeply than the antithetic faults. Either the antithetic faults formed earlier than the synthetic faults and have subsequently undergone more compaction, or the antithetic and synthetic faults formed contemporaneously and were subsequently rotated. We can discount the first hypothesis because some antithetic faults terminate onto synthetic faults, indicating that the antithetic faults must be younger. There are also examples of the opposite situation, where synthetic faults terminate onto antithetic faults, so we infer that synthetic and antithetic faults developed contemporaneously. Therefore we interpret the significantly gentler dips of the antithetic faults in comparison to the synthetic faults as being the result of simple shear (e.g. Ferrill et al., 1998). The interpretation of simple shear also explains why the fault dip of domino arrays of antithetic faults above Canyons I and II, and on the flanks of the Khop Structure become progressively smaller as the bedding dip increases: a greater amount of simple shear due to the downslope component of gravity acting on the overburden is to be expected where the bedding dip is greater.

The amount of displacement across the faulted interval due to simple shear may be estimated in the case of the aligned faults within Canyon III, where both antithetic and synthetic faults are

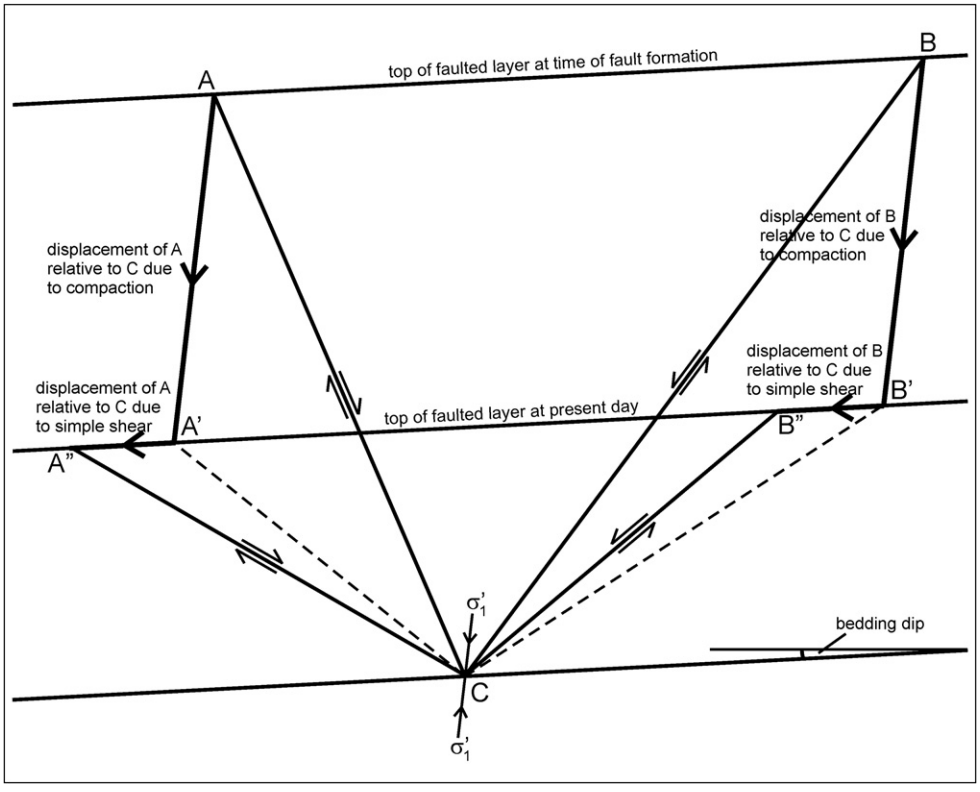

Fig. 15. Graphical illustration of the simple shear that has taken place across the faulted layer within Canyon III. Planar antithetic and synthetic faults are shown in vertical section, with bottom tips coincident at point C. In this diagram, the bedding plane through C is fixed. AC and BC are the original fault planes, inclined at angles of 30° to the direction of σ'_1 at the time of fault formation. A′C and B′C are the locations the fault planes would have had after compaction in the direction of σ'_1, which is parallel to lines AA′ and BB′, without simple shear. A″C and B″C are the fault planes at the present day: A″C dips at 30° from the horizontal, the observed average dip of antithetic faults; and B″C dips at 40°, the observed average dip of synthetic faults. Compaction is assumed to take place without any strain on bedding planes, so AB = A′B′ = A″B″. The lateral displacement across the faulted layer due to simple shear is estimated as the distance A″A′ = B″B′ ≈ 125 m, given that the present-day thickness of the faulted layer is ~300 m, so the amount of simple shear is ~23°.

present. The average dip of the antithetic faults is 30°, the average dip of the synthetic faults is 40°, and the thickness of the faulted interval is about 300 m. The dip of the strata within Canyon III is 3°, as in the case of the numerical example given at the end of Section 3. If we also assume that the constant $K = 0.7$, so that σ'_1 is inclined at 6.6° to the vertical (Section 3), and that the initial dips of the fault planes were at angles of 60 ± 6.6° (i.e. symmetrically disposed with respect to the direction of σ'_1), then we can estimate the displacement due to simple shear in the downslope direction. The calculation is a lengthy exercise in trigonometry, so we present the results in graphical form in Fig. 15. The lateral displacement across the faulted interval, of 300 m thickness, due to simple shear is approximately 125 m, corresponding to simple shear of approximately 23°. There are uncertainties in this estimate because we do not know the value of K, nor the initial dips of the antithetic and synthetic faults. Nevertheless, it seems reasonable to infer that the amount of simple shear that has taken place is around 20° or more.

8. Discussion and conclusion

The relationship between the canyons and the patterns of layer-bound compaction faulting on the Mauritanian continental margin is very clear (Figs. 8–11), with abrupt changes from polygonal arrays to linear arrays, which begs the question why such abrupt variations have not been reported before. A possible explanation lies in the relative sizes of fault spacing and canyon widths. The canyon widths on the Mauritanian continental margin are exceptionally large. On other margins, canyon widths may be less than the average fault length (e.g. Gay et al., 2004), and therefore would not be expected to exert a significant influence on fault patterns.

Layer-bound faults show strong alignment in regions where the bedding dip is greater than the average regional dip. Where they are aligned, the dip direction is largely controlled by the nature of the substrate. If the substrate is ductile and acts as a detachment, synthetic faulting is possible. Where the substrate is more rigid, the lower fault tips are pinned so that, kinematically, only antithetic faults can develop seismically resolvable throws. Mandl (1988) suggested that in the case of a sediment wedge, with a dipping upper surface and planar lower surface, that the orientation of σ'_1 will change with depth, rotating towards the pole to bedding near the base, favouring the development of antithetic faults towards the base. We discount this as a viable mechanism for the alignments reported here because the deformed unit is not a wedge but of uniform thickness and the entire sedimentary interval dips.

Where the bedding dip is 1–3°, the fault dips are not as would be expected considering the rotation of the principal stresses caused by the effect of downslope gravity traction. The dips of the antithetic faults dipping shelfwards are gentler than those of the synthetic faults dipping basinwards. We have interpreted the cause to be simple shear of around 20° or more, with the top of the layer hosting the polygonal faults having moved downslope by ~100 m or more relative to the bottom of the layer. This conclusion has potential implications for assessing the stability of continental margins. Systems of layer-bound compaction faults are not ubiquitous, but they are not the only possible strain markers available in seismic data for estimating simple shear. Fluid-escape features such as the pipes described by Berndt et al. (2003) are widespread across some parts of continental margins. If pipes have been active over long periods of geological time while sediments were being deposited, it may be possible to use their inclinations to estimate the amount of downslope simple shear that has taken place across different beds since their deposition.

Acknowledgements

We thank BG Group for funding MTI's PhD research; Tullow Oil and Petronas for permission to publish the seismic sections and maps in this study; and Jonny Imber, Simon Stewart and Alistair Chaney for discussions. Landmark Group Corporation provided the seismic interpretation software as part of the LGC University Grant Scheme. We thank Jonathan Turner and an anonymous reviewer for constructive comments.

References

Antobreh, A.A., Krastel, S., 2007. Mauritania slide complex: morphology, seismic characterisation and processes of formation. International Journal of Earth Sciences 96, 451–472.
Berndt, C., Bünz, S., Mienert, J., 2003. Polygonal Fault Systems on the Mid-Norwegian Margin: A Long-term Source for Fluid Flow. In: Geological Society, London, Special Publications, vol. 216, pp. 223–243.
Bishop, A.W., Green, G.E., Garga, V.K., Andresen, A., Brown, J.D., 1971. A new ring shear apparatus and its application to the measurement of residual shear strength. Geotechnique 21, 273–328.
Bonatti, E., 1976. Serpentinite protrusions in the oceanic crust. Earth and Planetary Science Letters 32, 107–113.
Bouma, A.H., 2004. Key Controls on the Characteristics of Turbidite Systems. In: Geological Society, London, Special Publications, vol. 222, pp. 9–22.
Brown, A., 2005. Interpretation of Three-Dimensional Seismic Data, sixth ed. AAPG and SEG, Tulsa.
Cartwright, J.A., 1994. Episodic basin-wide fluid expulsion from geopressured shale sequences in the North Sea basin. Geology 22, 447–450.
Cartwright, J.A., Dewhurst, D.N., 1998. Layer-bound compaction faults in fine-grained sediments. Geological Society of America Bulletin 110, 1242–1257.
Cartwright, J.A., Lonergan, L., 1996. Volumetric contraction during the compaction of mudrocks: a mechanism for the development of regional-scale polygonal fault systems. Basin Research 8, 183–193.
Carver, R.E., 1968. Differential compaction as a cause of regional contemporaneous faults. AAPG Bulletin 52, 414–419.
Clausen, J.A., Gabrielsen, R.H., Reksnes, P.A., Nysæther, E., 1999. Development of intraformational (Oligocene-Miocene) faults in the northern North Sea: influence of remote stresses and doming of Fennoscandia. Journal of Structural Geology 21, 1457–1475.
Cosgrove, J.W., 1999. Forced Folds and Fractures: An Introduction. In: Geological Society, London, Special Publications, vol. 169, pp. 1–6.
Crans, W., Mandl, G., Haremboure, J., 1980. On the theory of growth faulting: a geomechanical delta model based on gravity sliding. Journal of Petroleum Geology 2, 265–307.
Davies, R.J., Cartwright, J., 2002. A fossilized opal A to opal C/T transformation on the northeast Atlantic margin: support for a significantly elevated palaeogeothermal gradient during the Neogene? Basin Research 14, 467–486.
Davies, R.J., Ireland, M.T., Cartwright, J.A., 2009. Differential compaction due to the irregular topology of a diagenetic reaction boundary: a new mechanism for the formation of polygonal faults. Basin Research 21, 354–359.
Elvebakk, G., Hunt, D.W., Stemmerik, L., 2002. From isolated buildups to buildup mosaics: 3D seismic sheds new light on upper carboniferous-Permian fault controlled carbonate buildups, Norwegian Barents Sea. Sedimentary Geology 152, 7–17.
Ferrill, D.A., Morris, A.P., Jones, S.M., Stamatakos, J.A., 1998. Extensional layer-parallel shear and normal faulting. Journal of Structural Geology 20, 355–362.
Gay, A., Berndt, C., 2007. Cessation/reactivation of polygonal faulting and effects on fluid flow in the Vøring Basin, Norwegian Margin. Journal of the Geological Society 164, 129–141.
Gay, A., Lopez, M., Cochonat, P., Sermondadaz, G., 2004. Polygonal faults-furrows system related to early stages of compaction - upper Miocene to recent sediments of the Lower Congo Basin. Basin Research 16, 101–116.
Goulty, N.R., 2001. Polygonal fault networks in fine-grained sediments-an alternative to the syneresis mechanism. First Break 19, 69–73.
Goulty, N.R., 2002. Mechanics of layer-bound polygonal faulting in fine-grained sediments. Journal of the Geological Society 159, 239–246.
Goulty, N.R., 2008. Geomechanics of polygonal fault systems: a review. Petroleum Geoscience 14, 389–397.
Goulty, N.R., Swarbrick, R.E., 2005. Development of polygonal fault systems: a test of hypotheses. Journal of the Geological Society 162, 587–590.
Hansen, D.M., Shimeld, J.W., Williamson, M.A., Lykke-Andersen, H., 2004. Development of a major polygonal fault system in Upper Cretaceous chalk and Cenozoic mudrocks of the Sable Subbasin, Canadian Atlantic margin. Marine and Petroleum Geology 21, 1205–1219.
Hansen, J.P.V., Cartwright, J.A., Huuse, M., Clausen, O.R., 2005. 3D seismic expression of fluid migration and mud remobilization on the Gjallar Ridge, offshore mid-Norway. Basin Research 17, 123–139.
Higgs, W.G., McClay, K.R., 1993. Analogue Sandbox Modelling of Miocene Extensional Faulting in the Outer Moray Firth. In: Geological Society, London, Special Publications, vol. 71, pp. 141–162.

Hustoft, S., Mienert, J., Bunz, S., Nouzé, H., 2007. High-resolution 3D-seismic data indicate focussed fluid migration pathways above polygonal fault systems of the mid-Norwegian margin. Marine Geology 245, 89–106.
Kobayashi, K., Nakanishi, M., Tamaki, K., Ogawa, Y., 1998. Outer slope faulting associated with the western Kuril and Japan trenches. Geophysical Journal International 134, 356–372.
Lonergan, L., Cartwright, J., 1999. Polygonal faults and their influence on deep-water sandstone reservoir geometries, Alba Field, United Kingdom Central North Sea. AAPG Bulletin 83, 410–432.
Lonergan, L., Cartwright, J., Jolly, R., 1998. The geometry of polygonal fault systems in tertiary mudrocks of the North Sea. Journal of Structural Geology 20, 529–548.
Maltman, A., 1994. The Geological Deformation of Sediments. Chapman and Hall, London.
Mandl, G., 1988. Mechanics of Tectonic Faulting: Models and Basic Concepts. Elsevier, Amsterdam.
Mayne, P.W., Kulhawy, F.H., 1982. K_0-OCR relationships in soil. Journal of the Geotechnical Engineering Division, ASCE 108, 851–872.
Miyashiro, A., Shido, F., Ewing, M., 1969. Composition and origin of serpentinites from the mid-Atlantic ridge near 24° and 30° north latitude. Contributions to Mineralogy and Petrology 23, 117–127.
Morley, C.K., Guerin, G., 1996. Comparison of gravity-driven deformation styles and behavior associated with mobile shales and salt. Tectonics 15, 1154–1170.
Neagu, R.C., Cartwright, J., Davies, R., 2010. Measurement of diagenetic compaction strain from quantitative analysis of fault plane dip. Journal of Structural Geology 32, 641–655.
Reading, H.G. (Ed.), 1998. Sedimentary Environments: Processes, Facies and Stratigraphy. Blackwell Science, Oxford.
Riech, V., Roesch, H., 1977. Silica Diagenesis in Continental Margin Sediments off Northwest Africa. Initial Reports of the Deep Sea Drilling Project 41. Ocean Drilling Program. Texas A & M University, College Station, TX, pp. 879–905.
Santos, R.A., Lopes, M.R.F., Corá, C.A.G., Bruhn, C.H.L., 2000. Adaptive visualization of deepwater turbidite systems in Campos Basin using 3-D seismic. The Leading Edge 19, 512–517.
Schwab, A.M., Tremblay, S., Hurst, A., 2007. Seismic Expression of Turbidity-current and Bottom-current Processes on the Northern Mauritanian Continental Slope. In: Geological Society, London, Special Publications, vol. 277, pp. 237–252.
Stewart, S., 2006. Implications of passive salt diapir kinematics for reservoir segmentation by radial and concentric faults. Marine and Petroleum Geology 23, 843–853.
Stewart, S.A., Argent, J.D., 2000. Relationship between polarity of extensional fault arrays and presence of detachments. Journal of Structural Geology 22, 693–711.
Stroud, K.A., Booth, D.J., 2007. Advanced Engineering Mathematics, sixth ed. Palgrave Macmillan, Basingstoke.
Trabant, P., 1977. Synthesis of physical properties data from DSDP Leg 41. In: Gardner, J., Herring, J. (Eds.), Initial Reports of the Deep Sea Drilling Project, vol. 41, pp. 1199–1213.
Vear, A., 2005. Deep-water plays of the Mauritanian continental margin. In: Doré, A.G., Vinng, B.A. (Eds.), Petroleum Geology: North-West Europe and Global Perspectives–Proceedings of the 6th Petroleum Geology Conference. Geological Society, London, pp. 1217–1232.
Victor, P., Moretti, I., 2006. Polygonal fault systems and channel boudinage: 3D analysis of multidirectional extension in analogue sandbox experiments. Marine and Petroleum Geology 23, 777–789.
Watterson, J., Walsh, J., Nicol, A., Nell, P., Bretan, P., 2000. Geometry and origin of a polygonal fault system. Journal of the Geological Society 157, 151–162.